Geomechanics and Engineering, *Vol. 16, No. 6 (2018) 655-667*
DOI: https://doi.org/10.12989/gae.2018.16.6.655

Probabilistic stability analysis of rock slopes with cracks

J.Q. Zhu[1] and X.L. Yang*[2]

[1]Department of Civil and Architecture Engineering, Changzhou Institute of Technology, Jiangsu, China
[2]School of Civil Engineering, Central South University, Changsha, 410075, China

(Received April 28, 2018, Revised November 8, 2018, Accepted November 10, 2018)

Abstract. To evaluate the stability of a rock slope with one pre-exiting vertical crack, this paper performs corresponding probabilistic stability analysis. The existence of cracks is generally ignored in traditional deterministic stability analysis. However, they are widely found in either cohesive soil or rock slopes. The influence of one pre-exiting vertical crack on a rock slope is considered in this study. The safety factor, which is usually adopted to quantity the stability of slopes, is derived through the deterministic computation based on the strength reduction technique. The generalized Hoek-Brown (HB) failure criterion is adopted to characterize the failure of rock masses. Considering high nonlinearity of the limit state function as using nonlinear HB criterion, the multivariate adaptive regression splines (MARS) is used to accurately approximate the implicit limit state function of a rock slope. Then the MARS is integrated with Monte Carlo simulation to implement reliability analysis, and the influences of distribution types, level of uncertainty, and constants on the probability density functions and failure probability are discussed. It is found that distribution types of random variables have little influence on reliability results. The reliability results are affected by a combination of the uncertainty level and the constants. Finally, a reliability-based design figure is provided to evaluate the safety factor of a slope required for a target failure probability.

Keywords: rock slope; crack; probabilistic analysis; Hoek-Brown criterion; multivariate adaptive regression splines; response surface method

1. Introduction

Slope stability analysis plays a significant role in geotechnical engineering. In traditional stability analysis, the existence of cracks is generally ignored although they are widely found in either cohesive soil or rock slopes. Cracks introduce a discontinuity in both the static and kinematic fields, which results difficulties in calculating the collapse value of the slope when using some numerical methods like the finite element method (Li and Yang 2018c). The limit equilibrium method is normally employed in the existing research on the stability assessment for slope with cracks. However, this method is not rigorous and assumptions with respect to depth and location of cracks are usually required when performing such analyses. To overcome these difficulties, the limit analysis is adopted for stability analysis of soil slopes with pre-existing cracks (Li and Yang 2018d, Utili 2013, Michalowski 2013). However, there is rare research about stability analysis of rock slopes with cracks using limit analysis, in which the nonlinear failure criterion is employed to truly reflect the mechanical properties of rock masses. In this study, stability analysis combined with limit analysis for a rock slope with cracks, which is subjected to nonlinear Hoek-Brown (HB) criterion, is adopted as the deterministic computational model to predict slope stability.

Reliability method was used for estimating the safety of earth slopes in the 1970s. The randomness of strength parameters, geometry properties, and material properties can be taken into account in reliability methods, and accordingly designs based on these methods will be more rational and practical. Traditional probabilistic approaches include direct Monte Carlo simulation methods (MCS), classical first-order and second-order reliability methods (FORM/SORM). However, direct MCS is based on a lot of repeated calculations and it is inefficient when the original deterministic stability model is extremely complicated. As regards FORM/SORM, it is not suitable for high nonlinear limit-state function.

Recently, the response surface method (RSM) integrated with MCS is widely used in slope reliability analysis to reduce time costs without sacrificing the evaluation accuracy (Li and Yang 2018a, Xu *et al*. 2018, Yang and Liu 2018). A linear RSM is established to effectively approximate the finite element model of a homogenous slope. In order to deal with nonlinear stability problems, the quadratic response surface method (QRSM) was developed as an extension of linear RSM, and it was employed by several published studies (Li *et al*. 2016, Li and Chu 2015, Xu and Low 2006, Zhang *et al*. 2011). Base on QRSM, the stochastic response surface method (SRSM) using the Hermite polynomial chaos expansion can change the order of polynomial to adapt to high-dimensional problems, as shown in previous researches (Jiang *et al*. 2014, Pan and Dias 2018). However, QRSM and SRSM both are classified as parametric regression methods and they entail the prior assumption on the order and type of polynomials. To overcome the limitation of potentially assumptions for parametric regression methods, the multivariate adaptive

∗Corresponding author, Professor
E-mail: csuyang@aliyun.com

http://www.techno-press.org/?journal=gae&subpage=7
ISSN: 2005-307X (Print), 2092-6219 (Online)

regression splines (MARS) has been developed for soil slope system reliability analysis combined with limit equilibrium method, and it was also demonstrated that MARS fits high dimensional nonlinear problems better than QRSM and SRSM (Liu and Cheng 2016). The MARS has outstanding capacities to produce simple, easy-to-interpret and highly accurate models, to estimate the contributions of the input variables, and to compute highly efficient. The application of MARS to geotechnical engineering is a relatively recent development (Adoko *et al*. 2013, Zhang and Goh 2013), using limit equilibrium approach or numerical finite element method. However, how to combine MARS with limit analysis applied to rock slopes with pre-existing vertical cracks is a new issue.

This paper aims to perform probabilistic stability analysis of a rock slope of one pre-existing vertical crack by combining multivariate adaptive regression splines with the kinematic approach of limit analysis. The generalized HB criterion is adopted to depict the rock mass properties based on the equivalent friction angle (φ') and cohesive strength (c'). The φ' and c' can be obtained by HB parameters (σ_c, m_i and *GSI*) using the high nonlinear functions, as shown in Hoek *et al*. (2002). Addition, the factor of safety (*FoS*) is also a high nonlinear function with respect to friction angle when the limit analysis is adopted. This is because the friction angle exists in two parts of the *FoS* function, namely the tangent function and the exponent, as shown in appendix. Considering the high nonlinearity of these two parts, the *FoS* function is regarded as a high nonlinear function with respect to friction angle. The limit state function (LSF) is established based on *FoS*. Note that the HB parameters (σ_c, m_i and *GSI*) are regarded as the input parameters of LSF in this paper, and LSF is presented by the equivalent Mohr–Coulomb parameters for ease of use. Due to the two facts, LSF is apparently a complex nonlinear function. Therefore, the MARS is used to accurately approximate the LSF of a rock slope, and the reliability analysis is implemented by MARS-based MCS.

2. MARS

MARS is introduced as a flexible statistical strategy to represent the relationship between multivariate input variables and their dependent outputs. Liu and Cheng (2016) then developed the MARS for soil slope reliability analysis, and it was demonstrated that MARS fits high dimensional nonlinear problems better than conventional response surface methods, such as QRSM and SRSM. Considering that the stability analysis of rock slopes subjected to the HB criterion is high dimensional nonlinear, MARS is adopted in the following research.

Theoretically, MARS is defined as a regular combination of product splines, i.e., basis functions (BFs) based on piecewise polynomials. The number of BFs and the associated parameters with reference to each of them are automatically determined by the training data set, which is derived directly from the deterministic model. The relation between input (X) and output (Y) is expressed as

$$Y = a_0 + \sum_{m=1}^{M} a_m B_m(X) \tag{1}$$

Y is an approximation to a true function, which describes the deterministic model. $X=(x_1,x_2,\ldots,x_p)$ is the vector of input variables. a_m is the coefficient of the mth term in Eq. (1) obtained by the least squares method. $B_m(X)$ is the mth BF, which is expressed as

$$B_m(X) = \prod_{k=1}^{K_m} [s_{k,m} \times (x_{v(k,m)} - t_{k,m})]_+^q \tag{2}$$

where K_m is the number of $[s_{k,m} \times (x_{v(k,m)} - t_{k,m})]_+^q$. $[s_{k,m} \times (x_{v(k,m)} - t_{k,m})]_+^q$ is a two-sided truncated qth-order power function in the form of

$$[s_{k,m} \times (x_{v(k,m)} - t_{k,m})]_+^q = \max(0, s_{k,m} \times (x_{v(k,m)} - t_{k,m})^q) \tag{3}$$

where $[\cdot]_+$ means take the positive part; $s_{k,m}$ is the truncation direction with the value +1 or 1; $x_{v(k,m)}$ is the input variable that corresponds to the kth truncated qth-order power function; $t_{k,m}$ is the knot of the corresponding input variable $x_{v(k,m)}$; q is a non-negative parameter that is the power of truncated power function as shown in Eq. (3). It reflects a different degree of smoothness of the resulting MARS estimation. Piecewise cubic (q = 3) functions are used in this study. $B_m(X)$ may consist of a single truncated qth-order power function and two or more ones, which means that MARS can approximate highly nonlinear stability problems.

MARS is achieved by a two-step process, which is forward selection and backward pruning. At the beginning of the forward selection, there is only the basis function $B_0(X) = 1$ in the MARS model. Then a pair of BFs in which $s_{k,m}$ = 1 and $s_{k,m}$ = -1 respectively are introduced to the model, and adding BFs continues until the predefined maximum count of terms or the threshold of the training error is reached. As expected, the forward step finally generates a very complex and overfitting model, and the model consisting of large number of BFs may poorly predict other new points. To solve this overfitting problem, the backward pruning is required. In the backward step, the least effective BF in the current model will be deleted at each pruning step, and this trimming process is repeated until there is not BF available to be deleted. At each pruning step, a submodel is produced and a group of submodels are generated at the end of trimming process. Then, the efficiency of fit of each submodel is assessed according to generalized cross-validation (GCV). The optimum MARS model is identified as the submodel whose GCV is the lowest among the previously mentioned model subsets. GCV is defined as the mean-square residual error divided by a penalty dependent on the model complexity. For a training data set with N points, it is calculated as

$$\mathrm{GCV} = \frac{\frac{1}{N}\sum_{i=1}^{N}\left[y_i - Y(X_i)\right]^2}{\left[1 - \frac{M + d \times (M-1)/2}{N}\right]^2} \tag{4}$$

where M is the number of BFs; y_i is the true value at X_i; $Y(X_i)$ is the estimated value at X_i; and d is a penalizing factor and it is equal to three as a default value adopted in this study. The denominator is the penalty mentioned above which indicates the change of the model variance with regard to the model complexity.

3. Stability model of rock slope with pre-existing crack

3.1 Equivalent Mohr-Coulomb parameters based on Hoek-Brown criterion

Mohr-Coulomb soil parameters (c and φ) are required by most commercial software to analyze slope stability. However, the non-linear nature of the rock mass failure envelope is more pronounced at the low confining stresses, which is operational in stability problems (Li *et al*. 2012, Yang and Li 2018b, Yang and Li 2018c). As discussed by, the HB failure criterion is one of the few non-linear criteria utilized by geotechnical engineers to estimate rock mass strength (Li and Yang 2018b, Yang *et al*. 2018, Yang and Zhang 2018). The latest revised form of the HB criterion is presented as (Hoek *et al*. 2002)

$$\sigma_1 = \sigma_3 + \sigma_c\left(m\sigma_3 / \sigma_c + s\right)^n \tag{5}$$

where $\sigma 1$ is the maximum principal stress; σ_3 is the minimum principal stress; σ_c is the intact uniaxial compressive strength. m, s, and n are constants given by

$$m = m_i \exp\left(\frac{GSI - 100}{28 - 14D}\right) \tag{6}$$

$$s = \exp\left(\frac{GSI - 100}{9 - 3D}\right) \tag{7}$$

$$n = 0.5 + \left(e^{-GSI/15} - e^{-20/3}\right)/6 \tag{8}$$

where m_i is the material constant and D represents the disturbance degree of rock mass. As shown in the above equations, the magnitudes of m, s, and n are determined by geological strength index (GSI) and D.

For ease of use in most geotechnical engineering software still written in terms of the Mohr-Coulomb failure criterion, equivalent friction angles and cohesive strengths for each rock mass and stress range were developed by Hoek *et al*. (2002). Fig. 1 presents the relationship between the Hoek-Brown criterion and equivalent Mohr-Coulomb envelope. Hoek *et al*. (2002) deduced equivalent friction angle and cohesive strength by equalizing the areas above and below the Mohr–Coulomb plot over a range of minor principal stress value, which shown as

$$c' = \frac{\sigma_c\left[(1+2n)s + (1-n)m(\sigma_{3\max}/\sigma_c)\right]\left[s + m(\sigma_{3\max}/\sigma_c)\right]^{n-1}}{\sqrt{(1+n)(2+n)\left\{(1+n)(2+n) + 6nm\left[s + m(\sigma_{3\max}/\sigma_c)\right]^{n-1}\right\}}} \tag{9}$$

$$\varphi' = \arcsin\left\{\frac{6nm\left[s + m(\sigma_{3\max}/\sigma_c)\right]^{n-1}}{2(1+n)(2+n) + 6nm\left[s + m(\sigma_{3\max}/\sigma_c)\right]^{n-1}}\right\} \tag{10}$$

where $\sigma_{3\max}$ suggested by Hoek *et al*. (2002) as the following equation

$$\sigma_{3\max} = 0.72\sigma_{cm}\left(\sigma_{cm}/(\gamma H)\right)^{-0.91} \tag{11}$$

$$\sigma_{cm} = \sigma_c \frac{\left[m + 4s - n(m - 8s)\right](m/4 + s)^{n-1}}{2(1+n)(2+n)} \tag{12}$$

in which H is the height of the slope and γ is the material unit weight. For the slope stability problems, σ_{cm} can be determined by Eq. (12). According to the results using limit analysis, Li *et al*. (2008) found that using equivalent parameters could significantly overestimate safety for steep slopes. Therefore, Li *et al*. (2008) proposed that Eq. (11) should be modified as two separate equations shown as Eq. (13) and Eq. (14), respectively

$$\sigma_{3\max} = 0.2\sigma_{cm}\left(\frac{\sigma_{cm}}{\gamma H}\right)^{-1.07} \tag{13}$$

$$\sigma_{3\max} = 0.41\sigma_{cm}\left(\frac{\sigma_{cm}}{\gamma H}\right)^{-1.23} \tag{14}$$

3.2 Failure mechanism for rock slopes with vertical cracks

The log-spiral failure mechanism of rock slopes with

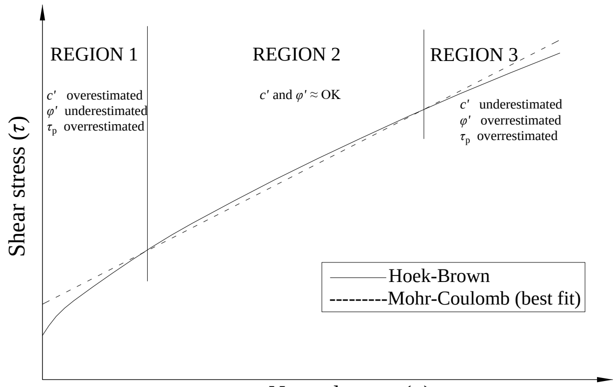

Fig. 1 Hoek-Brown and equivalent Mohr–Coulomb criteria adopted from Li *et al*. (2008)

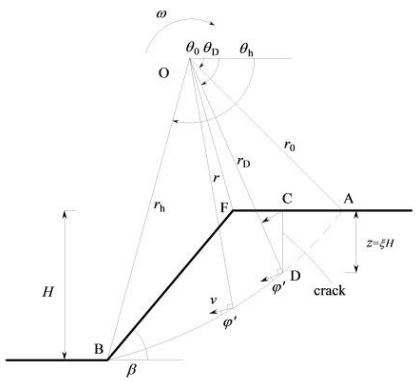

Fig. 2 Failure mechanism

pre-existing vertical cracks is illustrated in Fig. 2. The geometry of the failure mechanism is determined by the three geometrical parameters of θ_0, θ_D, and θ_h. The rotational failure surface is defined by the log-spiral equation, which is expressed as

$$r = r_0 e^{(\theta-\theta_0)\tan\varphi'} \tag{15}$$

where θ_0 is the geometric parameters; r is the radius of any point on the failure surface and it corresponds to θ; r_0 is the radius when $\theta=\theta_0$; and φ' is the equivalent friction angle.

Fig. 2 illustrates the failure model with the slope angle β, self-weight γ, and slope height H. The HB failure criterion is characterized by the equivalent cohesion c', and frictional angle φ'. A pre-existing vertical crack of unspecified location and depth is presented by line C-D, and the depth of the crack is $z=\xi H$, where ξ is the coefficient of crack depth. According to Utili (2013) and Yang and Li (2018), the coefficient of crack depth can be obtained by Eq. (16).

$$\xi = \frac{\sin\theta_c \cdot e^{(\theta_c-\theta_0)\tan\varphi'} - \sin\theta_0}{\sin\theta_h \cdot e^{(\theta_h-\theta_0)\tan\varphi'} - \sin\theta_0} \tag{16}$$

Michalowski (2013) proposed that the crack depth z should not be larger than the true maximum depth ($z_{\max}$) of a stable crack, and the $z_{\max}$ is limited by Eq. (17). In addition, it was concluded by Utili (2013) that departing from the slope face (line B-F) could not exist for the failure mechanisms with most critical over cracks of any depth and location cracks, which means cracks only could depart from the upper surface of the slope (A-F) .

$$z_{\max} = \frac{3.83c'}{\gamma}\tan\left(\frac{\pi}{4}+\frac{\varphi'}{2}\right) \tag{17}$$

3.3 Stability analysis using strength reduction technique

By using kinematical approach of limit analysis, an upper bound estimate of the slope height can be derived from equating the external work rate to the energy dissipation rate. The external force in this paper only involves the gravity force which results in the external work rate. The energy dissipation only includes the dissipation along the velocity discontinuity surface B-D. Note that energy is not dissipated along the crack C-D separating the two rock regions on both sides of C–D, and the block of falling rock C–D–B–F rotates away from the resting rock region A–C–D, as well as around a horizontal axis represented by point O. Therefore, the upper bound estimate of the slope height for a slope subjected to the HB criterion characterized by the equivalent cohesion and frictional angle is given by Eq. (18).

$$H = \frac{c'}{\gamma}\cdot f\left(\theta_0,\theta_D,\theta_h\right) \tag{18}$$

To estimate the stability of the slope with constant height, the *FoS* is adopted in this study, and the strength reduction technique is introduced to change the equivalent friction angle and cohesive strength by dividing *FoS* in Eq. (19).

$$\begin{cases} c_f = c'/FoS \\ \varphi_f = \arctan\left(\dfrac{\tan(\varphi')}{FoS}\right) \end{cases} \tag{19}$$

Substituting the reduced equivalent strength parameters (c_f and φ_f) to the right side of Eq. (18), and equating it to the constant height, the expression of *FoS* is obtained as

$$FoS = \frac{c'}{\gamma H} f\left(\theta_0,\theta_D,\theta_h\right) \tag{20}$$

where φ' in $f(\theta_0, \theta_D, \theta_h)$ of Eq. (18) has been replaced by φ_f. The minimal safety factor is obtained by minimizing Eq. (20) which is an implicit function with respect to three geometric variables, and this process is subjected to the following constraint conditions

$$s.t.\ \begin{cases} 0<\theta_0<\dfrac{\pi}{2} \\ \theta_0<\theta_D<\theta_h<\pi \end{cases} \tag{21}$$

When finding the minimum of *FoS*, the variables (θ_0, θ_D and θ_h) are changed sequentially in each computational loop. The procedure is repeated until the least upper bound solution is obtained. Then, the increments applied to the independent variables are reduced, and the process is repeated. The process is stopped when the increments used in optimization reached 0.01 for θ_0, θ_D and θ_h.

4. Probability analysis based on MARS-based MCS

4.1 Input random parameters for reliability analysis

Hoek (1998) introduced random parameters of HB criterion for rock mass into reliability analysis and discussed their influence on engineering design. Three input random variables, σ_c, m_i, and *GSI* are adopted. In the present analysis, the disturbance coefficient (D) is regarded as constant, as well as slope angle (β), unit weight (γ), and slope height (H).

Random variables are generally characterized by statistic properties which include mean value, standard deviation (SD), coefficient of variation (COV) and distribution type, which are presented in Table 1. The mean values listed in Table 1 for σ_c, m_i, and *GSI* are taken from a real slope reported by Douglas (2002) (Case 1A in Table 2). As shown in Pan and Dias (2017), three scenarios are introduced to investigate the influence of uncertainties of variables, i.e. COVs. The COVs of σ_c and m_i of optimistic scenario and pessimistic scenario are, respectively, obtained by reducing and increasing by 5% from those values of the neutral scenario, which is suggested in Hoek (1998). As regard *GSI*, coefficient of variation may be not suitable, since *GSI* is generally determined by geologists according to a given GSI chart, which means the estimated values of *GSI* should be within a small interval even evaluated by Table 1 Statistical properties for input random variables of

Case 1A

Input variables	Mean	COVs (%)			Distribution type
		Optimistic	Neutral	Pessimistic	
σ_c	3MPa	20	25	30	Normal/lognormal
m_i	25	7.5	12.5	17.5	Normal/lognormal
GSI	45	SD=2.5	SD=2.5	SD=2.5	Normal/lognormal

Table 2 Real slopes reported by Douglas (2002) (γ =25 kN/m^3, D=0.7)

Cases	σ_c (MPa)	m_i	*GSI*	H (m)	β (°)	Stable
1A	3	25	40-50	70	49	Yes
1B	3	25	40-50	41	50	No
1C	3	25	40-50	41	55	No
1D	3	25	40-50	46	49	No
1E	3	25	40-50	57	50	No
2A	5	25	50-60	58	50	Yes
2B	5	25	50-60	60	48	Yes
2C	5	25	50-60	60	52	Yes
3	5	7	50-60	38	39	Yes
4	150	19	70-80	200	65	Yes
5A	23	7	60-70	157	48	Yes
5B	23	7	60-70	60	53	Yes
6	25	7	40-50	110	48	No

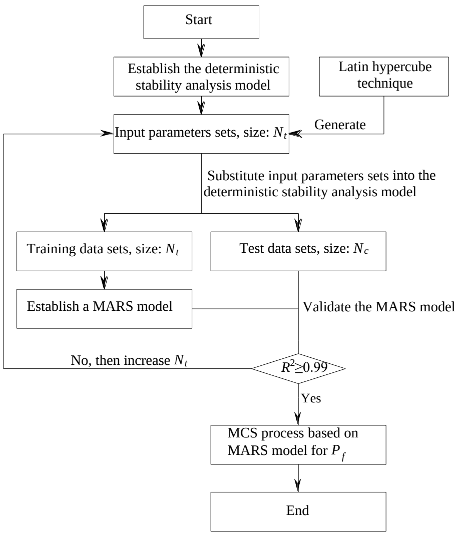

Fig. 3 Flowchart of MARS-based MCS program

different geologists. Therefore, the SD of 2.5 is adopted for representing the uncertainty of *GSI*, which is also a recommended value by Hoek (1998). The SD of *GSI* remains constant for three probabilistic scenarios.

Apart from random variables, constants are also should be determined for reliability analysis as input parameters. With respect to the value of disturbance coefficient D, it is set to 0.7 to represent modest rock mass damage in civil engineering as recommended by Hoek *et al*. (2002). Other constants β, γ, and H are shown as Case 1A in Table 2.

4.2 Application of MARS-based MCS method

The traditional MCS for slope reliability is directly based on the deterministic stability analysis model. However, if a deterministic model has high nonlinearity, such as the model adopted in this study due to nonlinear HB failure criterion, the complicated model will result in increasing time cost to obtain a *FoS* in Eq. (20) for given input parameters mentioned above. As a matter of fact, the progress of MCS is essentially repeated calculation for *FoS* and the number of repeating times is usually tens of thousands. To reduce the time cost of reliability, MARS method is introduced for establishing the highly consistent approximate relationship between *FoS* and input parameters, which is an explicit function consisting of BFs. The computation time for obtaining *FoS* will decrease. MARS-based MCS method can cost less time, and get more precise reliability results by improve repeating times.

Several steps are set to realize MARS-based MCS program for the reliability analysis of rock slopes with vertical cracks using limit analysis in conjunction with the equivalent Mohr–Coulomb parameters. First of all, prepare input parameters sets, which include N_t (N_t =300 as initial value) training samples generated by the Latin hypercube technique, and each sample consists of the values of three random variables and four constants mentioned above shown in Table 1. Second, substitute these input parameters into the deterministic stability analysis model, then N_t safety factors are obtained to get training data sets consisting of N_t safety factors and corresponding N_t generated training samples. The output is Y= (FoS_1, FoS_2,…,FoS_{Nt}), and the input is X=($\sigma_{c,1}$, $\sigma_{c,2}$,…, $\sigma_{c,\ Nt}$; $m_{i,1}$, $m_{i,2}$,…, $m_{i,\ Nt}$; GSI_1, GSI_2,…, GSI_{Nt}) in Eq. (1). In addition, test data sets are also prepared using the same method in the same two steps above and the size of test data sets is N_c= 200. Next, establish a MARS model using the training data sets and validate the MARS model using test data sets. The predictive ability of the MARS model is described by the coefficient of determination (R^2). If R^2 is greater than or equal to the predefined accuracy of 0.99, the established MARS model is considered to be suitable. Otherwise, the training sample size (N_t) should be increased and repeat the above-mentioned steps until an enough accurate model is obtained. Finally, the enough accurate MARS model is employed to execute MCS process and the failure probability (P_f) is obtained. The procedure of MARS-based MCS method mentioned above is presented by a flowchart in Fig. 3. In order to assess the failure probability of a rock slope with vertical crack, the limit state function is defined as

$$G = FoS - 1 \tag{22}$$

where the *FoS* can be estimated by instituting samples of three random variables into MARS model. The failure probability can be evaluated by

$$P_f = \frac{1}{N}\sum_{i=1}^{N} I(G) \tag{23}$$

where N = number of samples of random variables for MCS. $I(G)$=1 for G < 0, otherwise $I(G)$=0. The estimation accuracy of P_f is assessed by the coefficient of variation of

P_f as

$$\mathrm{COV}_{P_f} = \sqrt{(1-P_f)/(NP_f)} \tag{24}$$

It can be easily found that the coefficient of variation of P_f is highly dependent on the size of samples, since ten times better accuracy need one hundred times size of samples. However, the direct Monte Carlo sampling technology is completely random and samples are more likely to be drawn from distributions with high probability of occurrence, which may result in ignoring samples with low probability of occurrence when the size of samples is not enough. These two reasons lead to high-precision reliability results requiring a large number of samples, which eventually results in increased time costs. The Latin hypercube technique is adopted to generate samples accurately reflecting probability distributions without ignoring samples with low probability of occurrence and can reduce the number of Monte Carlo samples, which is set to 10^6 in this study for enough estimation accuracy of P_f.

5. Results and discussions

This section discusses the influence of distribution types, level of uncertainty level, and constants on the probability density functions of *FoS* and failure probability. A reliability-based design figure is obtained for rock slopes with vertical cracks. All calculations consider independent variables.

5.1 Influence of distribution types

As stated previously, three random variables (σ_c, m_i, and *GSI*) are adopted for reliability analysis of rock slopes with pre-existing vertical cracks, and statistical properties of input random variables presented in Table 1 are used in this section. Distribution types of random variables comprise of normal and lognormal distribution for strength parameters. Although Hoek (1998) introduced normal distributions of σ_c, m_i, and *GSI*, using a lognormal distribution can ensure positive values of strength parameters to guarantee physical meaning. This part focuses on influence of these two distributions on results of reliability analysis. Chen and Dai (2011) also proved that these two distributions were more suitable than other types of distribution according to the maximum entropy principle.

Fig. 4 and 5 illustrate the influence of distribution types of three random variables on distributions of safety factors presented by curves of probability density function (PDF), and the influence on the probability of failure (P_f), respectively. P_f can be read by the ordinate of a point whose abscissa equal to *FoS*=1 in cumulative distribution function (CDF). In Fig. 4, the shapes of the safety factor distributions are similar to Gaussian distribution and the difference between two curves is negligible, as well as in Fig. 5. According to reliability analysis based on MARS-based MCS, P_f for normal distribution and lognormal distribution are 8.23% and 6.26%, respectively, which also can be found in Fig. 5. It can be seen that the influence of distribution types of three random variables on reliability results is non-significant, and normal distribution results in relatively conservative P_f. In the following research, normal distribution is adopted for reliability analysis.

Fig. 6 presents the comparison between *FoS* predicted by MARS and those calculated by the deterministic model under different distribution types for case 1A. The

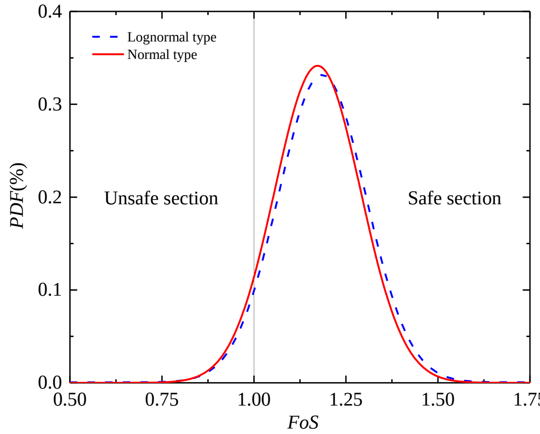

Fig. 4 Influence of distribution types on probability density functions

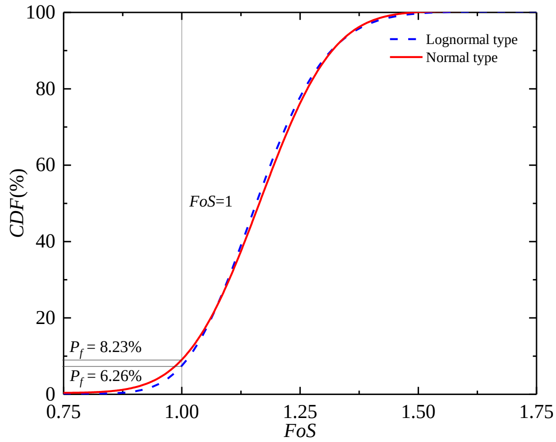

Fig. 5 CDF curves for different distribution types

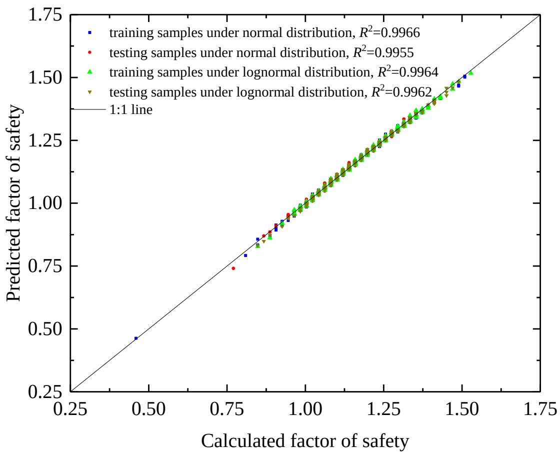

Fig. 6 Comparison between *FoS*s predicted by MARS and *FoS*s calculated by the deterministic model in case 1A

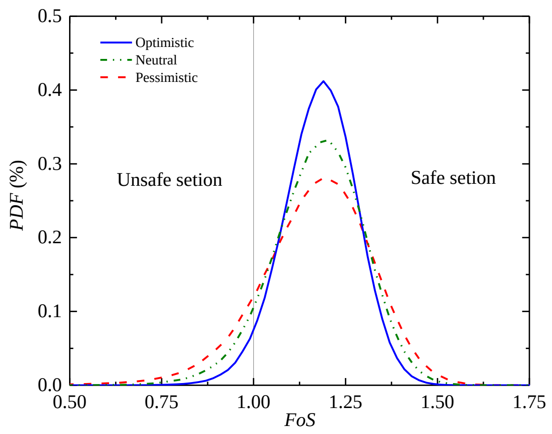

Fig. 7 Influence of uncertainty level (COVs) on probability density functions for slope height H_1

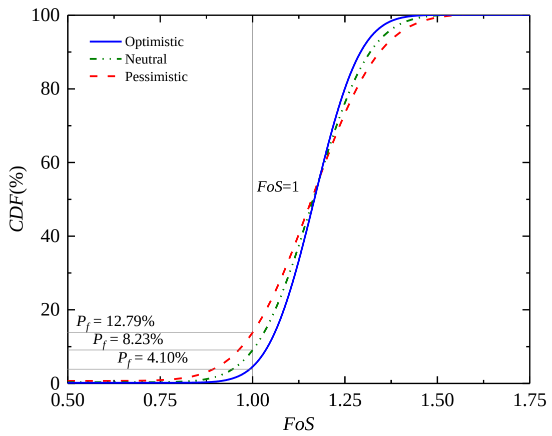

Fig. 8 CDF curves of the slope whose height is H_1 under different uncertainty level (COVs)

coefficient of determination (R^2) is adopted to estimate the predictive ability of the MARS model. As presented in Fig. 6, R^2 is extremely close to 1 and points locate nearly at the line with 1:1 slope, which means MARS model has high precision to simulate the implicit relation between *FoS* and input parameters under either normal distribution or lognormal distribution.

5.2 Influence of uncertainty level

Uncertainty level presented by coefficients of variation (COVs) of random variables is mainly considered in reliability analysis. In this section, three scenarios mentioned above are studied for reliability analysis. The influence of uncertainty level (COVs) on probability density functions of *FoS* is presented in Fig. 7. For all curves of optimistic, neutral and pessimistic scenarios, an apparent trend is that the distribution of the safety factor becomes wider and lower as the values of COVs increase, i.e., more pessimistic, but the mean of safety factor is nearly constant. This trend causes the augmentation of the proportion of left side of the vertical line which means *FoS*<1, while COVs increase. This change finally results in an increase in unsafe area and therefore P_f increases. As shown in Fig. 8, P_f for optimistic, neutral and pessimistic

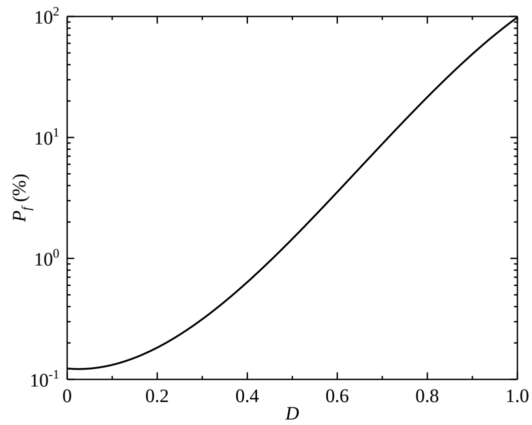

Fig. 9 Influence of disturbance coefficient (D) on P_f

Table 3 P_f(%) for different disturbance levels (Ds)

D=0.1	D=0.3	D=0.5	D=0.7	D=0.9
0.14	0.32	1.38	8.23	55.55

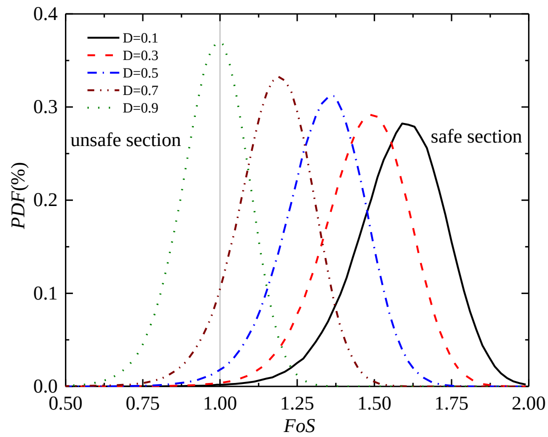

Fig. 10 Influence of disturbance coefficient (D) on probability density functions for neutral scenario

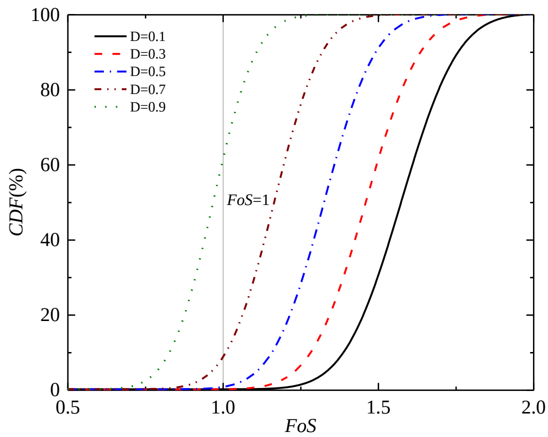

Fig. 11 CDF curves for disturbance coefficients (Ds) for neutral scenario

scenarios are 4.10%, 8.23% and 12.79% respectively. It can be conducted that COVs can significantly influence reliability results by changing the shape of PDF curves for *FoS*.

5.3 Influence of constants

Although studying random variables is predominant in probability analysis, it is still worthy of investigating the influence of disturbance factor (D), and geometric parameters of slope height (H), and slope angle (β) on the P_f evaluations. In the following section, these three constants are researched for rock slopes with pre-existing vertical cracks.

As shown in Table 3 and Fig. 9, P_f increases significantly while D only enlarges a little. This phenomenon can be explained by Fig. 10 and 11. In Fig. 10, a noticeable trend is that the distribution of the safety factor becomes narrower and higher as the value of D increases, and the mean of safety factor becomes lower, which manifests as moving left of *PDF* curves. In Fig. 11, changes of the shape of *PDF* curves lead to bigger slopes of *CDF* curves, and lower mean of safety factor also results in moving left of *CDF* curves. Finally, P_f increases significantly with little changing of D.

The change law of P_f with respect to slope height under different uncertainty levels is presented in Fig. 12. For each scenario, P_f increase slowly at low values of height and then the growth rate gradually increases. When P_f reaches approximately 50%, the increasing speed reaches a maximum, and then the growth rate gradually slows down,

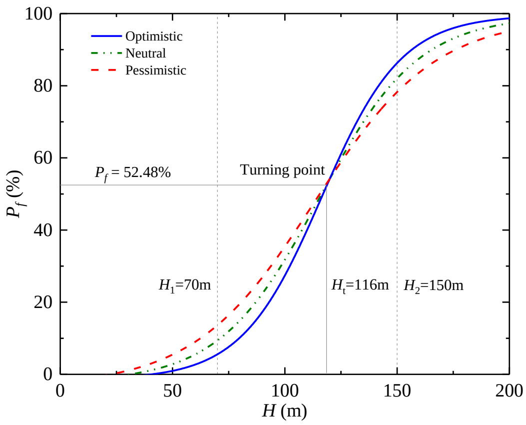

Fig. 12 The change law of P_f with respect to slope height under different uncertainty levels

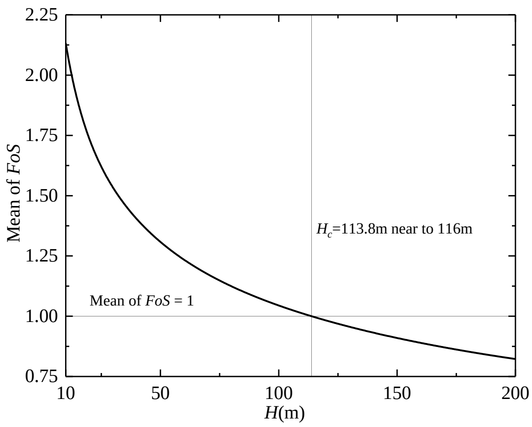

Fig. 13 The change law of mean of *FoS* with respect to slope height for neutral scenario

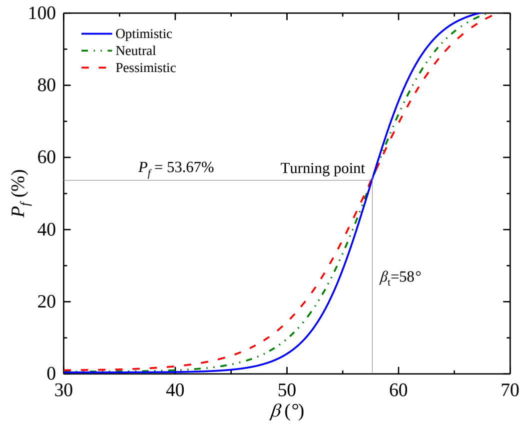

Fig. 14 The change law of P_f with respect to slope angle under different uncertainty levels

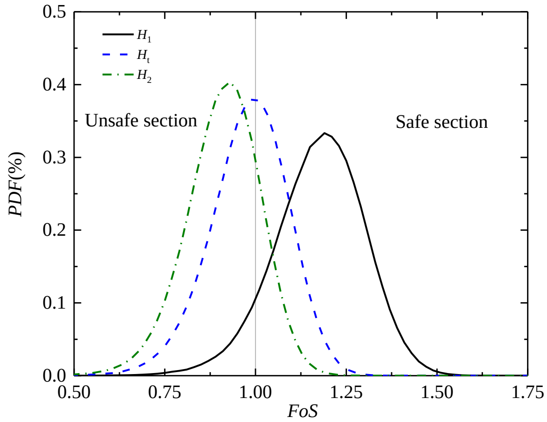

Fig. 15 Influence of slope height (H) on probability density functions for neutral scenario

Table 4 P_f (%) for different slope heights under three uncertainty levels (COVs)

Slope height	Optimistic	Neutral	Pessimistic
H_1	4.10	8.23	12.79
H_t	52.48	52.48	52.48
H_2	85.39	81.26	77.69

and the final curve appears as an S-shape. The turning point is worth noting, since the three curves begin to change slope at the same turning point. For all scenarios, P_f is close to 50% at the turning point, and the corresponding slope height is 116m. With respect to the influence of slope height on mean of *FoS*, it is presented in Fig. 13. From the above discussion, it can be seen that the uncertainty level does not affect the mean value of *FoS*, so Fig. 13 only shows the variation law of *FoS* with slope height for neutral scenario. Obviously, mean of *FoS* decreases with increasing slope height. Let mean of *FoS* equal to 1, and the critical height (H_c) is obtained, which is usually used to get a dimensionless stability factor in deterministic stability analysis, and it is equal to 113.8m near to the slope height at the turning point. Therefore, considering differences between reliability analysis and deterministic stability analysis, the slope height at the turning point can be regarded as the critical slope height.

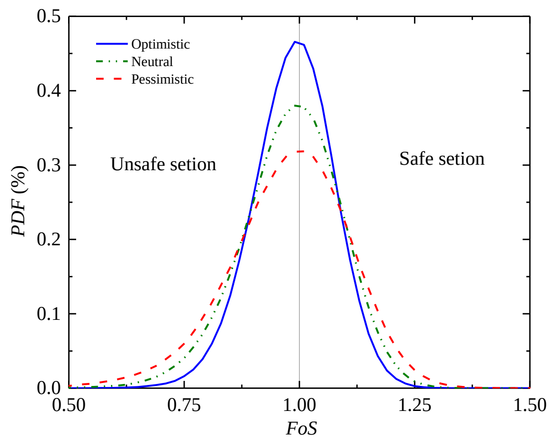

Fig. 16 Influence of uncertainty level (COVs) on probability density functions for slope height H_t

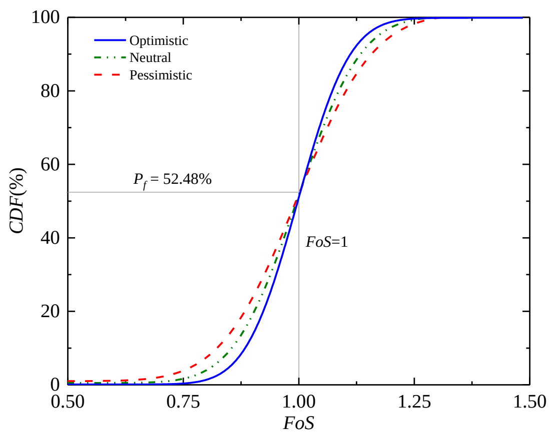

Fig. 17 CDF curves of the slope whose height is H_t under different uncertainty level (COVs)

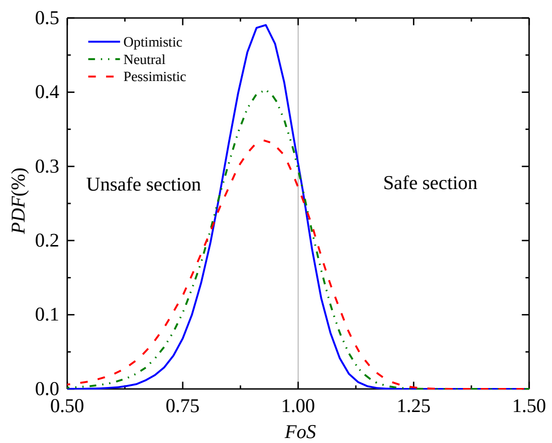

Fig. 18 Influence of uncertainty level (COVs) on probability density functions for slope height H_2

It is an interesting phenomenon that the turning point is inconsistent with the above finding that different COVs can significantly influence reliability results (i.e., P_f in this study). To explain this phenomenon, two specific values on behalf of slope heights lower and higher than the critical slope height respectively, i.e., H_1=70 m and H_2=150 m respectively, are used, as shown in Fig. 12. It is shown in

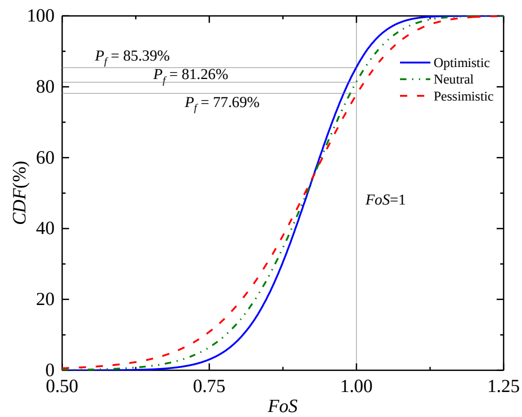

Fig. 19 CDF curves of the slope whose height is H_2 under different uncertainty level (COVs)

Table 4 that the variation rule of P_f corresponding to the slope height at different uncertain levels is not the same. Specifically, for H_1, P_f increases with COV, whereas this change is reversed for H_2, and P_f does not change with COV for the critical slope height at the turning point. The reason can be found by observing PDF and CDF curves corresponding to three kinds of slopes with different heights mentioned above. From Figs. 7, 16 and 18, a common trend for PDF curves is that higher COVs lead to wider and lower curves causing the augmentation of the proportion of left and right marginal areas between curve and abscissa, while the mean of *FoS* is nearly constant. In Fig. 7, the slope height is less than the critical slope height, so the mean of *FoS* is bigger than 1, which means increasing COV can aggrandize the area between the curve and the abscissa in the unsafe part while the whole area is regarded as one dimensionless unit, therefor P_f increases as COV increases as shown in Fig. 8. For slope height bigger than critical slope height, the mean of *FoS* is less than 1 as presented in Fig. 18, therefor a smaller COV can improve failure risk of slopes by decreasing the area between the curve and the abscissa in the safe part, which can be observed in Fig. 19. However, P_f of a critical rock slope is close to 50% and fluctuates little as COV changes, since the PDF curve of the safety factor is nearly symmetrical with respect to the critical vertical line (i.e., *FoS*=1), as shown in Fig. 16 and Fig. 17. In addition, the influence of slope height (H) on probability density functions for neutral scenario is presented in Fig. 15. An observed trend is that the distribution of the safety factor becomes a little narrower and higher as the slope height increases, and the mean safe factor decrease.

With respect to slope angle β, the change law of P_f under different uncertainty levels is presented in Fig. 14. Obviously, there is also a turning point corresponding to the critical slope angle, and the change law of P_f with respect to slope angel is the same as the slope height. It is deserved pointed out that P_f corresponding to turning point is equal to 53.67% which is also near to 50% as the same as the turning point with respect to the critical slope height.

In summary, the reliability results are affected by a combination of the uncertainty level that affects *PDF* shape and the constants that affect the value of the mean of *FoS*.

In addition, it should be pointed out that the uncertainty level presented by the coefficient of variation has a significant influence on the reliability-based design for geotechnical engineers because of the guarantee of safety, i.e., *FoS*>1. According to reliability analysis above, the uncertainty level should be realistic to get a more reliable result in reliability-based design for geotechnical engineering. To avoid either overestimating or underestimate security of rock slopes with pre-existing vertical cracks, extensive and accurate geotechnical experiments should be conducted before reliability-based design implementation to obtain the realistic uncertainty level in reliability analysis. However, in most cases, the necessary conditions for conducting tedious geotechnical tests are lacking, so the COV and SD values proposed by Hoek (1998), namely neutral scenario, can be used as reference values which is adopted in the following research.

5.4 Reliability-based design

In this section, 13 cases of real rock slopes in Table 2 are taken for reliability analysis, and the influence of pre-existing vertical cracks of unspecified location and depth is considered. Table 2 lists details of each slope, including HB criterion parameters (m_i, GSI, and σ_c), slope geometry (β and H), and stable or unstable state. These cases were reported by Douglas (2002). Because no information about rock mass unit weight γ and disturbance factor D is reported, D is equal to 0.7 and γ is set to 25 kN/m^3. The uncertainty level of three random variables is assumed to be the neutral scenario which is suggested by Hoek (1998), and they are independent and subject to normal distribution to gain conservative solutions. The mean values of variables m_i and σ_c are taken from Table 2; the mean value of GSI is equal to the average value of its interval. The comparison of computed failure probabilities for all slopes between previous research (Li *et al*. 2012) and this study is provided in Table 5.

It can be seen in Table 5 that the failure risk of all cases compared to previous reliability results obtained by Li *et al.* (2012) will be higher when considering the existence of cracks but the failure probabilities in all cases are of the same order of magnitude, therefore the results are reasonable. But it also should be pointed out that the degree of influence of cracks on reliability results is not uniform. For example, the difference of reliability result for case 2B reaches up to 56.7%, but the difference for case 1C is only 0.8%. For the reported stable cases (2A, 2B, 2C, 3, 4, 5A and 5B), P_f values obtained are all smaller than 0.15% and bigger than 0.006%. In addition, case 1A is table but has relatively high P_f therefor the slope is under critical conditions, even if it is recorded as stable, which is also found in Li *et al*. (2012). For the reported unstable cases (1B, 1C, 1D, 1E and 6), P_f values obtained are all bigger than 0.9%.

To apply reliability analysis into design of rock slopes with pre-existing vertical cracks, mean slope safety factor (FoS_u) corresponding to failure probability derived from MARS-based MCS method can be considered as a reasonable index to estimate stability and safety degree of slopes. Fig. 20 presents the relation between failure probability and FoS_u for three cases of different uncertainty levels of input parameters. Obviously, the turning point also exists at FoS_u=1 corresponding to the critical slope height or the slope angle. In order to give a safe enough FoS_u for a conservative design, a reasonable reference value of P_f =0.00723% is adopted as shown in Fig. 20, which is put forward by Pan and Dias (2017). The safety factor required for a target failure probability can be directly got from the curves shown in Fig. 20. For example, with respect to the optimistic case, FoS_u=1.59 is required for suggested failure probability of 0.00723%. For the neutral uncertainty level, the reasonable FoS_u is approximately 1.88. However, for the pessimistic scenario, it is impossible to get a reasonable FoS_u in the considered range of safety factor. So, the FoS_u of 1.88 can be considered as a reference value for geotechnical engineering.

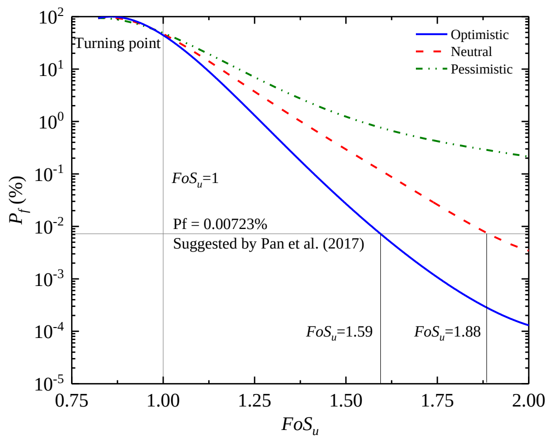

Fig. 20 Failure probability as a function of the mean safety factor

Table 5 Comparison of obtained P_f(%) for 13 cases of real rock slope

Cases	Li *et al*. (2012)	This study	Difference (%)	Stable
1A	6.74	8.23	22.1	Yes
1B	0.83	0.9989	20.3	No
1C	3.93	3.9629	0.8	No
1D	1.04	1.3373	28.6	No
1E	3.74	4.36	16.6	No
2A	0.0571	0.0677	18.6	Yes
2B	0.0457	0.0716	56.7	Yes
2C	0.1014	0.1316	29.8	Yes
3	0.0943	0.1234	30.9	Yes
4	0.0052	0.0062	19.2	Yes
5A	0.046	0.057	23.9	Yes
5B	0.0171	0.0178	4.1	Yes
6	0.966	0.9775	1.2	No

6. Conclusions

The stability of rock slope with one pre-existing vertical crack of unspecified location and depth is investigated in the framework of probability theory. The deterministic stability analysis of rock slope with crack is based on the upper bound method, and the equivalent Mohr–Coulomb parameters based on the HB criterion are adopted to characterize the rock mass strength. In order to estimate the stability of the slope with constant height, the *FoS* which is derived from strength reduction technique is used in this study. Three input random variables are σ_c, m_i, and *GSI*. The disturbance coefficient *D* is regarded as a constant, as well as slope angle, unit weight, and slope height. The MARS for rock slope reliability analysis is used to establish the highly consistent approximate relationship between *FoS* and three input random parameters, which can greatly improve the computational efficiency of MCS. The influence of distribution types, level of uncertainty level, and constants on the probability density functions of *FoS*, and failure probability is discussed in this study. Conclusions can be drawn as:

• The shapes of *FoS* distributions corresponding to normal distribution and lognormal distribution are similar and the difference between two curves is negligible. Therefore, the influence of distribution types of three random variables on reliability results is non-significant, and the normal distribution results in relatively conservative P_f.

• For three random variables consisting of σ_c, m_i, and *GSI*, more pessimistic uncertainty level can only result the *PDF* curve of the *FoS* wider and lower, but the mean of *FoS* is nearly constant. For constants including disturbance factor *D*, geometric parameters of slope height *H*, and slope angle β, it is found that P_f increases significantly with little changing of *D* and the variation rule of P_f corresponding to the slope height at different uncertain levels is not the same. All constants can change the value of the mean of *FoS*. Therefore the reliability results are affected by a combination of the uncertainty level and the constants. A turning point in *PDF* and *CDF* curves is found, and it is considered as a critical point corresponding to *FoS*=1. Pre-exiting vertical cracks can reduce reliability of rock slopes, which leads to higher failure probabilities than that of slopes without cracks, but the failure probabilities for both are of the same order of magnitude.

• To apply reliability analysis into design of rock slopes with pre-existing vertical cracks, FoS_u corresponding to failure probability is considered as a reasonable index to estimate stability and safety degree of slopes. The relationship between FoS_u and P_f is displayed in Fig. 20. The values of COVs of random variables should be determined by sufficient experimental and field measured data, if no further sample and data information is available. Geotechnical engineers can adopt the curve based on the uncertainty level suggested by Hoek (1998), namely the neutral scenario. According to a reasonable reference value of P_f =0.00723%, the FoS_u=1.88 can be considered as a reference value for geotechnical engineering.

References

Adoko, A.C., Jiao, Y.Y., Wu, L., Wang, H. and Wang, Z.H. (2013), "Predicting tunnel convergence using multivariate adaptive regression spline and artificial neural network", *Tunn. Undergr. Sp. Technol.*, **38**(3), 368-376.

Chen, X.W. and Dai, W. (2011), "Maximum entropy principle for uncertain variables", *Int. J. Fuzzy Syst.*, **13**(3), 232-236.

Douglas, K.J. (2002), "The shear strength of rock masses", Ph.D. Dissertation, The University of New South Wales, Sydney, Australia.

Hoek, E. (1998), "Reliability of Hoek-Brown estimates of rock mass properties and their impact on design", *Int. J. Rock Mech. Min. Sci.*, **35**(1), 63-68.

Hoek, E., Carranza-Torres, C. and Corkum, B. (2002), "Hoek-Brown failure criterion-2002 Edition", *Proceedings of the NARMS-TAC Conference*, Toronto, Canada, July.

Jiang, S.H., Li, D.Q., Zhang, L.M. and Zhou, C.B. (2014), "Slope reliability analysis considering spatially variable shear strength parameters using a non-intrusive stochastic finite element method", *Eng. Geol.*, **168**(1), 120-128.

Li, A.J., Cassidy, M.J., Wang, Y., Merifield, R.S. and Lyamin, A.V. (2012), "Parametric Monte Carlo studies of rock slopes based on the Hoek-Brown failure criterion", *Comput. Geotech.*, **45**, 11-18.

Li, A.J., Merifield, R.S. and Lyamin, A.V. (2008), "Stability charts for rock slopes based on the Hoek-Brown failure criterion", *Int. J. Rock Mech. Min. Sci.*, **45**(5), 689-700.

Li, D.Q., Zheng, D., Cao, Z.J., Tang, X.S. and Phoon, K.K. (2016), "Response surface methods for slope reliability analysis: Review and comparison", *Eng. Geol.*, **203**, 3-14.

Li, L. and Chu, X. (2015), "Multiple response surfaces for slope reliability analysis", *Int. J. Numer. Anal. Meth. Geomech.*, **39**(2), 175-192.

Li, T.Z. and Yang, X.L. (2018a), "Probabilistic stability analysis of subway tunnels combining multiple failure mechanisms and response surface method", *Int. J. Geomech.*, **18**(12), 04018167.

Li, Y.X. and Yang, X.L. (2018b), "Three-dimensional seismic displacement analysis of rock slopes based on Hoek-Brown failure criterion", *KSCE J. Civ. Eng.*, **22**(11), 4334-4344.

Li, Z.W. and Yang, X.L. (2018c), "Active earth pressure for soils with tension cracks under steady unsaturated flow conditions", *Can. Geotech. J.*, **55**(12), 1850-1859.

Li, Z.W. and Yang, X.L. (2018d), "Stability of 3D slope under steady unsaturated flow condition", *Eng. Geol.*, **242**, 150-159.

Liu, L.L. and Cheng, Y.M. (2016), "Efficient system reliability analysis of soil slopes using multivariate adaptive regression splines-based Monte Carlo simulation", *Comput. Geotech.*, **79**, 41-54.

Michalowski, R.L. (2013), "Stability assessment of slopes with cracks using limit analysis", *Can. Geotech. J.*, **50**(10), 1011-1021.

Pan, Q.J. and Dias, D. (2018), "Probabilistic analysis of a rock tunnel face using polynomial chaos expansion method", *Int. J. Geomech.*, **18**(4), 04018013.

Utili, S. (2013), "Investigation by limit analysis on the stability of slopes with cracks", *Geotechnique*, **63**(2), 140-154.

Xu, B. and Low, B.K. (2006), "Probabilistic stability analyses of embankments based on finite-element method", *J. Geotech. Geoenviron. Eng.*, **132**(11), 1444-1454.

Xu, J.S. and Yang, X.L. (2018), "Three-dimensional stability analysis of slope in unsaturated soils considering strength nonlinearity under water drawdown", *Eng. Geol.*, **237**, 102-115.

Yang, X.L. and Li, Z.W. (2018a), "Factor of safety of three-dimensional stepped slopes", *Int. J. Geomech.*, **18**(6), 04018036.

Yang, X.L. and Li, Z.W. (2018b), "Kinematical analysis of 3D passive earth pressure with nonlinear yield criterion", *Int. J. Numer. Anal. Meth. Geomech.*, **42**(7), 916-930.

Yang, X.L. and Li, Z.W. (2018c), "Upper bound analysis of 3D static and seismic active earth pressure", *Soil Dyn. Earthq. Eng.*,

108, 18-28.
Yang, X.L. and Liu, Z.A. (2018), "Reliability analysis of three-dimensional rock slop", *Geomech*. *Eng*., **15**(6), 1183-1191.
Yang, X.L. and Zhang, S. (2018), "Risk assessment model of tunnel water inrush based on improved attribute mathematical theory", *J*. *Central South Univ*., **25**(2), 379-391.
Yang, X.L., Zhou, T. and Li, W.T. (2018), "Reliability analysis of tunnel roof in layered Hoek-Brown rock masses", *Comput*. *Geotech*., **104**, 302-309.
Zhang, J., Zhang, L.M. and Tang, W.H. (2011), "New methods for system reliability analysis of soil slopes", *Can*. *Geotech*. *J*., **48**(7), 1138-1148.
Zhang, W.G. and Goh, A.T.C. (2013), "Multivariate adaptive regression splines for analysis of geotechnical engineering systems", *Comput*. *Geotech*., **48**(3), 82-95.

CC

Appendix

$$\frac{H}{r_0} = \sin\theta_h \, e^{(\theta_h - \theta_0)\tan\varphi'} - \sin\theta_0 \tag{A1}$$

$$\frac{L_1}{r_0} = \frac{\sin(\theta_h - \theta_0)}{\theta_h} - \left\{\sin\theta_h \, e^{(\theta_h - \theta_0)\tan\varphi'} - \sin\theta_0\right\} \frac{\sin(\theta_h + \beta)}{\sin\beta \sin\theta_h} \tag{A2}$$

$$\frac{L_2}{r_0} = \frac{\sin(\theta_D - \theta_0)}{\theta_D} - \left\{\sin\theta_D \, e^{(\theta_D - \theta_0)\tan\varphi'} - \sin\theta_0\right\} \frac{\cos\theta_D}{\sin\theta_D} \tag{A3}$$

$$f\left(\theta_0, \theta_D, \theta_h\right) = \frac{f_d}{f_1 + f_2 + f_3 - p_1 - p_2 - p_3} \times \frac{H}{r_0} \tag{A4}$$

$$f_d = \frac{e^{2\tan\varphi'(\theta_h - \theta_0)} - e^{2\tan\varphi'(\theta_D - \theta_0)}}{2\tan\varphi'} \tag{A5}$$

$$f_1 = \frac{\left(3\tan\varphi' \cos\theta_h + \sin\theta_h\right) e^{3(\theta_h - \theta_0)\tan\varphi'} - 3\tan\varphi' \cos\theta_0 - \sin\theta_0}{3(1 + 9\tan^2\varphi')} \tag{A6}$$

$$f_2 = \frac{1}{6}\frac{L_1}{r_0}\sin\theta_0\left(2\cos\theta_0 - \frac{L_1}{r_0}\right) \tag{A7}$$

$$f_3 = \frac{1}{6} e^{(\theta_h - \theta_0)\tan\varphi'} \left[\sin(\theta_h - \theta_0) - \frac{L_1}{r_0}\sin\theta_h\right] \cdot \left(\cos\theta_0 - \frac{L_1}{r_0} + e^{(\theta_h - \theta_0)\tan\varphi'} \cos\theta_h\right) \tag{A8}$$

$$p_1 = \frac{\left(3\tan\varphi' \cos\theta_D + \sin\theta_D\right) e^{3(\theta_D - \theta_0)\tan\varphi'} - 3\tan\varphi' \cos\theta_0 - \sin\theta_0}{3(1 + 9\tan^2\varphi')} \tag{A9}$$

$$p_2 = \frac{1}{6}\frac{L_2}{r_0}\sin\theta_0\left(2\cos\theta_0 - \frac{L_2}{r_0}\right) \tag{A10}$$

$$p_3 = \frac{1}{3} e^{2(\theta_D - \theta_0)\tan\varphi'} \cos^2\theta_D \cdot \left\{e^{(\theta_D - \theta_0)\tan\varphi'} \sin\theta_D - \sin\theta_0\right\} \tag{A11}$$